Two-Phase Flow Regimes of Condensing R-134a at Low Mass Flux in Rectangular Microchannels

Michael A. VANDERPUTTEN[a] , Tabeel A. JACOB[a], Maria SATTAR[b], Nouman ALI[b], and Brian M. FRONK[a] [c]

[a] School of Mechanical, Industrial and Manufacturing Engineering, Oregon State University
Corvallis, OR 97331 USA

[b] U.S.-Pakistan Center for Advanced Studies in Energy (USPCAS-E), National University of Sciences and Technology, Islamabad, Pakistan

[c]Corresponding author: Phone: +1-541-737-3952 E-mail: brian.fronk@oregonstate.edu

Abstract

Qualitative two-phase flow regime data are obtained from high-speed visualization of condensing flows of R-134a at mass fluxes from 75 to 150 kg m^{-2} s^{-1} and quality from 0.1 to 0.8 in square microchannels (D_H = 0.84 mm) cooled from a single side. Superheated R-134a is distributed into multiple parallel microchannels and then partially condensed, using a counterflow water loop, to the desired quality prior to the inlet of a visualization section. This experimental arrangement mitigates the potential for flow maldistribution. Despite very small heat duties, a low uncertainty in the quality in the visualization section is maintained by enforcing a large temperature difference on the water-side (ΔT > 10 K). For all conditions, annular or annular/wavy type flow were observed, with no distinct intermittent flow. Data are compared with flow macro and mini/microchannel maps, which are shown to over predict the occurrence of intermittent or wavy flow.

Keywords

Condensation, flow regime, visualization, two-phase flow, refrigerant

Highlights

- Flow visualization of two-phase refrigerant condensation at low mass fluxes

- Data compared with flow maps designed for condensing refrigerants

- Disagreement between flow maps and data and with one another

NOMENCLATURE

c	Specific heat (J kg^{-1} K^{-1})
D	Diameter (m)
D_H	Hydraulic diameter (m)
Fr	Froude number (-)
g	Acceleration due to gravity (m s^{-2})
G	Mass flux (kg m^{-2} s^{-1})
h	Specific enthalpy (J kg^{-1})
H	Channel height (m)
$j_\text{v}{}^*$	Dimensionless vapor velocity from [1] (-)
$\dot{m}$	Mass flow rate (kg s^{-1})
P	Pressure (Pa)
P_r	Reduced pressure (-)
$\dot{Q}$	Heat duty (W)
Re	Reynolds number (-)
Su_V	Suratman number (-), $Su_\text{V} = \rho_V \sigma D / \mu_V^2$
T	Temperature (K)
U	Uncertainty (varies)
v	Specific volume (m^3 kg^{-1})
W	Channel width (m)
We	Weber number (-)
x	Thermodynamic equilibrium quality (-)
X_tt	Turbulent-turbulent Martinelli parameter (-)

Greek Letters

ρ	Density (kg m^{-3})
μ	Dynamic viscosity (kg m^{-1} s^{-1})

σ Surface tension (N m^{-1})

Subscripts

L   Liquid phase

r   Refrigerant

w   Water

V   Vapor phase

1. Introduction and Prior Work

Predicting condensation two-phase flow regimes and the associated heat transfer and pressure drop in microchannels is critical for designing advanced heating, cooling, and refrigeration systems. It is well established that at small hydraulic diameters, the two-phase flow morphology deviates from that predicted for larger tubes at equivalent operating conditions. Namely, the importance of gravity dominated flow regimes including stratified and wavy flow decrease, while the preponderance of intermittent, slug-and-plug type flow increases [2–6]. In addition, it has been shown that flow maps and transition criteria developed for air/water flows do not yield good predicative capability for low surface tensions fluids such as R-134a [7].

Understanding the prevailing flow regime for condensing refrigerants is important for developing mechanistic models to predict heat transfer and pressure drop. In an attempt to characterize condensation flow regimes, there have been numerous qualitative and quantitative studies using high-speed visualization, capacitance, and other measurement techniques. Doretti et al. [8] provided a review of condensation flow patterns inside plain and microfin tubes (all sizes), and found wide scatter in the data despite a large volume of archival literature. For small channels, flow regime visualization for condensation of refrigerants is even more limited [4,5,7]. On the other hand, boiling/evaporation studies of flow regimes of refrigerants in mini/microchannels are more prevalent [9,10]. However, caution should be used when extrapolating these results to condensation, as the flow regimes are influenced by the heating boundary condition. This is particularly true for boiling/evaporation where nucleating bubbles can be confined within mini/microchannels.

Most of the available work of mini/microchannel flow regime mapping has focused on adiabatic, air/water flows at relatively high superficial velocities or condensing/evaporating refrigerants, at large mass fluxes ($G > 150$ kg m^{-2} s^{-1}). While these mass fluxes may be realistic for high-flux electronics cooling (i.e., short flow lengths), they are not representative of the flow conditions for high heat duty microchannel condensers in heating, cooling, and power generation. These applications are generally characterized by

heat exchangers with multiple parallel microchannels with relatively low mass flux to effectively transfer heat while minimizing frictional pressure loss [11].

Thus, the objective of this study was to investigate flow regimes and the predictive capability of different flow maps for condensing refrigerants in small channels at low mass fluxes. Qualitative flow regime data were obtained from high-speed visualization of condensing flows at nominal mass fluxes from 75 to 150 kg m^{-2} s^{-1} for a quality from 0.1 to 0.8 of R-134a in parallel rectangular microchannels ($D_H = 0.84$ mm). Initially, superheated R-134a was distributed into multiple parallel microchannels and then condensed to the desired quality prior to the inlet of a visualization section. This experimental arrangement mitigates the potential for flow maldistribution and provides a more realistic simulation of what would happen inside an actual condenser. Despite the very small heat duties, a low uncertainty in the inlet quality is maintained by enforcing a large temperature difference on the water-side ($\Delta T > 10$ K). Finally, the data were compared to flow regime maps from the literature.

R-134a was chosen as a working fluid due to its prevalence in the HVAC&R industry and the availability of prior work using this fluid. R-134a is in the process of being phased down due to its high global warming potential (GWP). However, the thermophysical properties are comparable to new low GWP replacements such as R-1234yf and R-513A, providing some confidence that the results of this study can be extended to new refrigerants.

1.1 Two-Phase Flow Regime Maps

Prior flow regime experiments have led to the creation of empirical and semi-empirical maps to predict flow regimes, which can then be used to inform the development of mechanistic heat transfer and pressure drop models. The low mass flux data obtained in this study are compared to five different flow maps. Of these, four were specifically developed for condensing refrigerants.

The classic Taitel and Dukler [12] flow map for horizontal and inclined round tubes is still commonly used as the basis for many contemporary flow maps. The semi-theoretical work attempted to predict flow

transitions by considering flow regime stability, and proposed conditions for which each regime might remain stable or transition. The model neglects the effects of fluid surface tension, not originally pertinent for the relatively larger sizes of tubes considered.

Cavallini et al. [1] developed a flow map based on a database of flow visualization and heat transfer data of condensing refrigerants. They concluded that there exists a dimensionless vapor velocity (j_v^*), above which all flow will be annular and below which transition to either stratified, intermittent, or stratified annular will be determined by a constant turbulent-turbulent Martinelli parameter (X_{tt}). The flow map developed in their study was combined with a heat transfer model to predict local condensation heat transfer coefficient. It was tuned using over 600 data points and compared with a 10.4% mean absolute deviation to a total of 1,778 data points from a variety of sources. The model is estimated to be applicable for tubes with diameters from 3.0 to 21.0 mm, reduced pressures less than 0.75, and liquid/vapor density ratios over 4.

Drawing on a flow boiling two-phase transition map originally proposed by Kattan et al. [13], a study presented by El Hajal et al. [14] proposed a new flow map for condensation in round horizontal tubes. A database of 425 data points comprising six different refrigerants and a variety of test conditions ($D = 8$ mm, $0.12 < x < 0.88$, $65 < G < 750$ kg m^{-2} s^{-1}) was statistically fit to the flow transition model proposed in earlier works for boiling flows. The El Hajal et al. [14] map predicts transitions between stratified, wavy, intermittent, annular, mist, and dispersed flow. The proposed flow map was also shown in a subsequent study [15], which made use of the map to predict condensation heat transfer, to be able to well predict the heat transfer in data produced by nine independent laboratories. It is reported to be applicable to a wide range of conditions ($3.14 < D_H < 21.4$ mm, $16 < G < 1532$ kg m^{-2} s^{-1}, $0.02 < P_r < 0.8$, $76 < (We/Fr)_L < 884$).

Kim and Mudawar [16] proposed a flow regime transition model for condensing flows in small channels based on a heat transfer database of 923 data points in mini/microchannels from 8 different sources. They developed transition criteria based on a modified Weber number and Martinelli parameter.

The method was based on a wide variety of geometries ($0.89 < D_h < 4.18$ mm, circular and non-circular) and fluids (R-22, R-32, R-134a, R-404A, R-410A, CO_2).

Nema et al. [17] developed dimensionless transition criteria for condensing refrigerants. The study drew from an extensive R-134a database ($1 < D_H < 4.91$ mm, $150 < G < 750$ kg m^{-2} s^{-1}) and dimensional transition criteria originally proposed by Coleman and Garimella [4]. The flow map proposed by Nema et. al. [17] uses the Martinelli parameter, Bond number, Weber number, and dimensionless variable T proposed by Taitel and Dukler [12] to predict flow regimes in micro and macro channels. The map uses a critical Bond number to determine a transition criterion from large to small tubes, where surface tension effects begin to play a greater role in the observed flow regimes. The prediction of the model scales with the flow geometry to include the relative effects of shear and body forces on the flow. The microscale regimes predicted below the critical Bond number are dispersed, annular, intermittent, and mist.

2. Experimental Approach

An experimental facility was developed to produce and measure low mass flux, two-phase flows of low surface tension fluids at varying thermodynamic quality with a maximum pressure of 2070 kPa (300 psia). Figure shows a schematic of the complete facility with important refrigerant thermodynamic state points labeled.

2.1 Test Section Design

The test section (shown in Figure 2) condensed superheated vapor to a specified thermodynamic quality, and then allowed optical access to the two-phase flow. The fluid enters the test section as a superheated vapor and is distributed to the multiple parallel channels. Unlike many other multi-phase visualization studies [18–20], where flow enters the test section as a two-phase mixture, superheating the inlet fluid enables a more uniform distribution. The refrigerant is then condensed to the desired quality in the pre-condensing length of the flow channels by water flowing in counterflow from the bottom side (see Figure 2a).
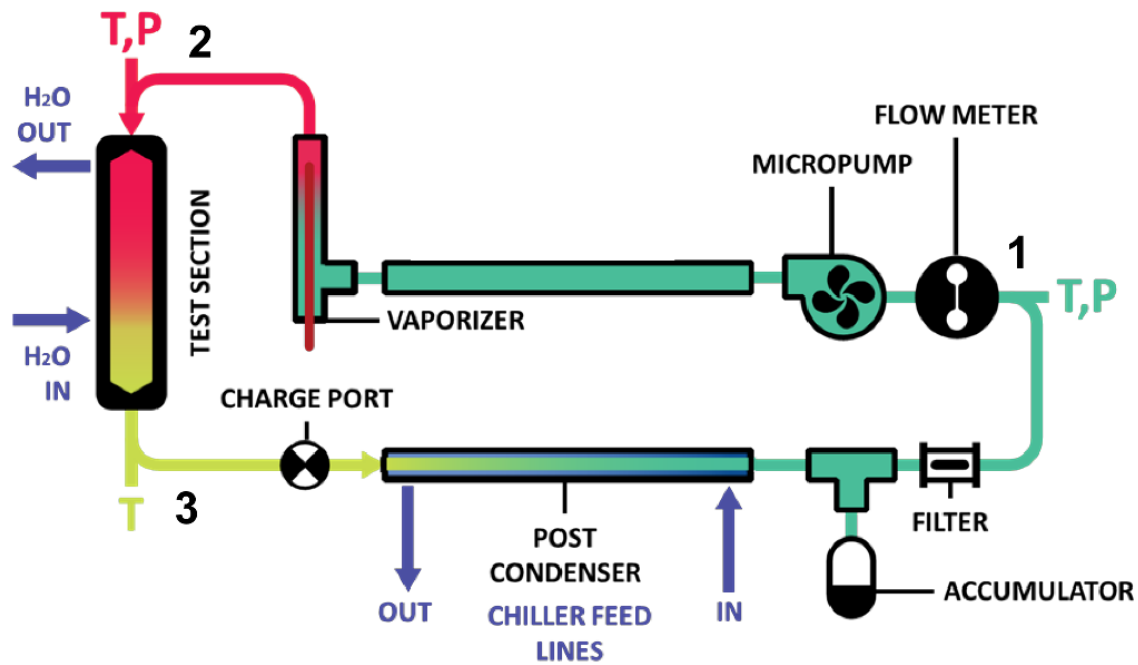
Figure 1: Schematic of experimental facility with state points labeled

The microchannel heat exchanger plate consisted of five, rectangular (average aspect ratio = 0.92) parallel microchannels in Aluminum 6061. The heat exchange plate was machined on a Fadal VMC15 vertical milling center and the as-machined dimensions of the channels were verified using a ZeScope^{TM} optical profiler. The ZeScope^{TM} measures surfaces using vertical scanning interference microscopy, which enables it to resolve three-dimensional features as small as 2 μm. The width and depth of each channel was measured using this technique, with results shown in Table 1. The average measured channel hydraulic diameter was 842.49 μm, with a standard deviation of 1.1%. A hydraulic dimeter of under 1.0 mm was desired to maintain a Confinement number below the microscale transition predicted by the literature [21].

An impact resistant polycarbonate was selected for the viewing plate material. With a reported thermal conductivity of 0.19 W m^{-1} K^{-1}, the 9.5 mm thick polycarbonate sheet had orders of magnitude higher thermal resistance than the 1.0 mm thick aluminum heat exchange plate, mitigating the risk of substantial heat loss from the test section. For similar reasons, Delrin® (Polyoxymethylene) was selected for the base plate material, which houses the cooling fluid channel and supports the heat exchange plate. A neoprene O-
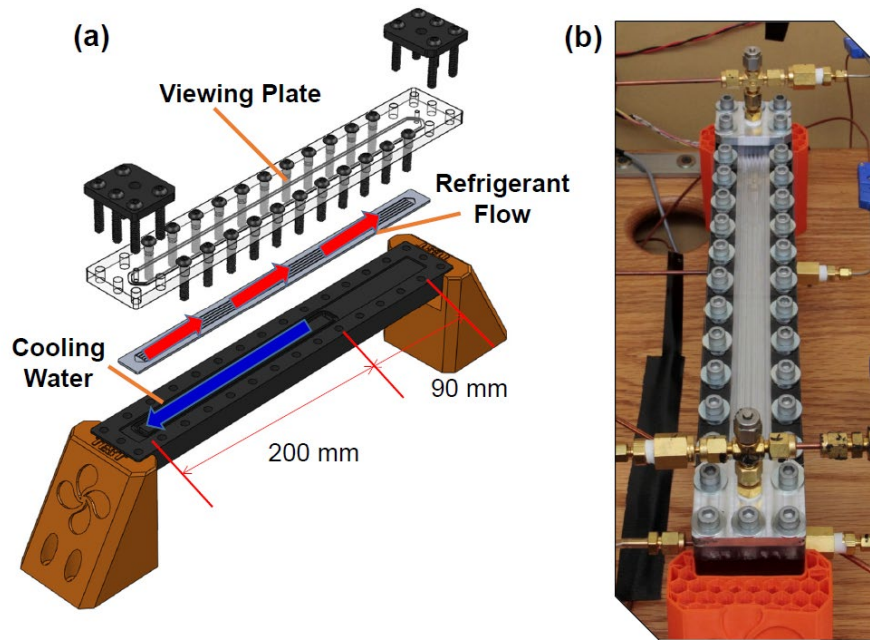
Figure 2: (a) Schematic of test section and (b) photograph of uninsulated test section

ring cord was used to seal the heat exchange plate against the base plate to contain the cooling fluid. Lastly, to incorporate NPT ports for the inlet and outlet of the working fluid, 12.7 mm (0.5 inch) thick plates were added at both ends of the test section to integrate the flow inlet and exit NPT fittings. A 0.5 inch diameter O-ring was used to seal the face of the NPT blocks to the viewing section. The blocks were machined from aluminum for ease of tapping the NPT ports and maintaining a face seal near the O-ring. The system was insulated with 5 mm thick aerogel material with a thermal conductivity of 0.274 W m^{-1} K^{-1} to minimize heat loss wherever optical access to the flow was not required.

Table 1: Microchannel test section dimensions

	Height (μm)	Width (μm)	D_H (μm)	Aspect Ratio
1	897.93	809.89	851.64	0.902
2	844.45	810.39	827.07	0.960
3	866.76	810.87	837.88	0.936
4	880.94	810.76	844.39	0.920
5	898.51	809.05	851.44	0.900

2.2 Refrigerant and Water Loops

At state point one (Figure 1), the temperature and pressure of the refrigerant are known, and can be used to determine the fluid density entering the flowmeter. To achieve mass fluxes in the range of 75 to 150 kg m^{-2} s^{-1} through the five channels of the test section, the required flow rate of liquid R-134a at the pump and flowmeter ranged from approximately 13 to 25 mL min^{-1}. A positive displacement gear pump was used to provide this flow rate. The pump head is designed such that no lubricating grease or oil contacts any internal flow components, which are driven via a magnetic drive. Because of the replaceable gearing in the system, wide ranges of low mass flow rates are achievable, even with a low viscosity refrigerant. The pump is driven via a magnetic coupling by a brushless 20 to 30 V variable speed motor that is controlled by a 0 to 5 V signal. Both the supply and signal voltages are provided by a variable voltage supply unit capable of 0.01 V variations.

From the pump, the fluid enters the vaporizer, which consists of a 250 W in-line cartridge heater controlled by a Variac variable voltage controller. A K-type thermocouple was included in the heater tip to ensure the surface temperature was maintained below 250°C (maximum operating temperature was 760°C). From the vaporizer, superheated refrigerant entered the test section where it was partially condensed and visualized, described in the following sections. After exiting test section at state 3 (in Figure 1), the two-phase mixture was then fully condensed in a counterflow tube-in-tube post-condenser before returning to the gear pump. A nitrogen charged piston accumulator was used to maintain the desired saturation pressure.

Heat was rejected from the test section to a closed loop of circulating deionized water. Because the thermocouples used to measure the water temperature have an uncertainty of ±0.5°C, a large temperature difference is required on the water-side to keep uncertainty low in the energy balance used to calculate the condensation heat duty. To maintain high water-side temperature difference a combination of low water flow rate and low inlet temperature were required. To provide the desired flow rates, a set of NE-1010 New Era Pump Systems syringe pumps were used (flow rate ±1% of setpoint). The two syringe pumps are able

to communicate with each other and can operate in continuous flow mode with one pump filling as the other discharges. The two 60 mL syringes were connected to a water reservoir by a set of one-way valves, and then fed into the water-side pre-chiller. The circulating deionized water and the post-condenser were cooled by a NESLAB M75 circulating chiller.

2.3 Instrumentation

Water and refrigerant temperatures were measured with T-type thermocouples inserted into the flow. The thermocouples were calibrated in a heated drywell and ice bath against a high accuracy Fluke platinum resistance thermistor. Refrigerant pressure was measured at the pump and test section inlet (state points one and 2) using Omega PX209-300Al absolute pressure transducers. The transducers used have a measurable range of 0-2070 kPa (0-300 psia) and a reported uncertainty of ±2.59 kPa. Because R-134a is a low viscosity, low surface-tension fluid it is challenging to pump and meter at low flow rates. To measure flow rates in the 13-25 mL min^{-1} range, a nutating flowmeter from DEA Engineering was used. The flowmeter has a dual chamber flow path that allows liquid to pass through only by displacing the nutating metering element. The nutating flowmeter is capable of measuring low-viscosity flows from 1-250 mL min^{-1} and has a rated max operating pressure of 20.7 MPa (3,000 psia) with a nominal uncertainty of $\pm1.0\%$ of reading. The water-side volumetric flow rate was directly measured from the New ERA syringe pump controller, with a reported uncertainty of $\pm1.0\%$ of reading.

A Phantom V310 high speed camera was used to capture optical images of the flow. A 60mm Nikon AF Micro Nikkor^{TM} lens was used to capture a 1280 x 800 pixel resolution image of the viewing section. Because frames were captured at 2400 fps with a 415.96 µs exposure time, a large amount of system light was required. Two 120 W EnergySaverLED^{TM} lights were used to illuminate the test section channels. The LED lights are capable of producing 13,000 lumens with minimal heat generation.

3. Experimental Methods and Analysis

3.1 Data Collection and Analysis

To capture each data point, the refrigerant and cooling water flow rates were adjusted until the desired state point was reached. After temperature fluctuations were within ±0.5°C for a minimum of five minutes, the system was determined to be at steady state and data capture was started. Temperature, pressure, and fluid flow rate measurements were collected using a LabVIEW [22] program developed to receive information from the DAQ system. Data was collected at a rate of 1 Hz for a minimum of 4 minutes. The Phantom PCC software provided with the Phantom camera was used to collect the visualization footage. Images and video of each data point were exported from the .cine raw files into more manageable video and image files for comparison.

For the analysis, all R-134a thermodynamic properties were calculated using built-in functions in *Engineering Equation Solver* [23], which used the fundamental equation of state by Tilner-Roth and Baehr [24]. For each point, the refrigerant mass flow rate was found by multiplying the measured volumetric flow rate by the liquid density (found as a function of the temperature/pressure). To calculate the visualization section quality, an energy balance was first performed on the pre-condensing portion of the test section to determine the refrigerant condensation heat duty:

$$\dot{Q}_r = \dot{Q}_w + \dot{Q}_{loss} \tag{1}$$

The water-side heat duty was calculated by Eq. (2).

$$\dot{Q}_w = \dot{m}_w \cdot c_w \cdot \left(T_{w,out} - T_{w,in}\right) \tag{2}$$

Heat losses were estimated by developing relations for the overall heat transfer coefficient (*UA*) from each fluid stream to the ambient. Single-phase flow tests for the range of temperature and flow rates expected in the study were conducted separately for both water and the refrigerant. The change in fluid temperature was measured and used to calculate the heat loss and overall *UA*. For both streams, the heat transfer resistance is dominated by the conductive resistance through the heat exchanger body material and insulation, and the natural convection and radiation from the insulated surface. This was confirmed by the

heat loss tests as the measured *UA* at different flow rates were within experiments uncertainty of one another. Thus, these tests effectively establish a thermal resistance from each fluid stream to the ambient that is independent of the fluid flow rate (and each fluids' associated convective heat transfer coefficient). The average *UA* for the 10 water-side tests was $UA_w = 0.095$ W K^{-1}, and for the 16 refrigerant tests was $UA_r = 0.138$ W K^{-1}. Thus, the total heat loss/gain term was calculated according to Eq. (3), where the log-mean temperature difference is between the measured fluid and ambient temperatures. A conservative uncertainty of ±25% for the value of *UA* was assumed for the uncertainty propagation discussed in Section 3.2. The average calculated heat loss was 10.3% of the measured condensation heat duty for the 40°C experiments, and 16% for the 55°C experiments. Data with heat loss greater than 25% were excluded from the results reported in this study. Heat loss was greater for the higher saturations temperatures, and at high outlet qualities, where the condensation heat duty was relatively small.

$$\dot{Q}_{loss} = \dot{Q}_{loss,w} + \dot{Q}_{loss,r}$$

where

$$\dot{Q}_{loss,w} = UA_w \cdot \Delta T_{LM,w}$$
$$\dot{Q}_{loss,r} = UA_r \cdot \Delta T_{LM,r}$$

(3)

The refrigerant enthalpy into the test section (h_2) was calculated from the measured temperature and pressure, the enthalpy at the inlet of the visualization section (h_3) was determined by Eq. (4).

$$h_3 = h_2 - \frac{\dot{Q}_r}{\dot{m}_r}$$

(4)

Finally, the thermodynamic quality in the visualization section was found as a function of the calculated enthalpy h_3, and the local measured saturation temperature.

3.2 Uncertainty Analysis

A critical challenge in this experiment was maintaining low uncertainty in the calculated thermodynamic quality at relatively low mass fluxes. The uncertainty in each measured system variable (temperature/pressure/flow rate) included systematic uncertainty associated with the instrument itself (U_0,

temperature ±0.5°C, pressure ±2.59 kPa, water and refrigerant volumetric flow rates ±1% of reading, as reported by manufacturer), uncertainty from the DAQ, U_1, (including uncertainty from quantization, internal zero reference and cold-junction compensation), and random uncertainty, U_2, from the measurement variability. The total uncertainty for each measurement was found using the RMS method $\left(U_x = \sqrt{U_0^2 + U_1^2 + U_2^2} \right)$ to determine a final measurement uncertainty in each data reading. A detailed discussion of the calculation of each of these parameters is provided in VanderPutten [25]. For each data point collected, the propagated uncertainty in the calculated quality and mass flux were determined using the Kline-McClintock [26] method, as shown below in Eq. (5).

$$U_G = \sqrt{\left(\frac{\partial G}{\partial x_1} U_1 \right)^2 + \left(\frac{\partial G}{\partial x_2} U_2 \right)^2 + ... + \left(\frac{\partial G}{\partial x_n} U_n \right)^2} \qquad (5)$$

Uncertainties in the mass flux parameter were an average of ±4%, with a maximum of ±7%. For the thermodynamic quality, the absolute uncertainty was an average of ±0.03, with a maximum value of ±0.06.
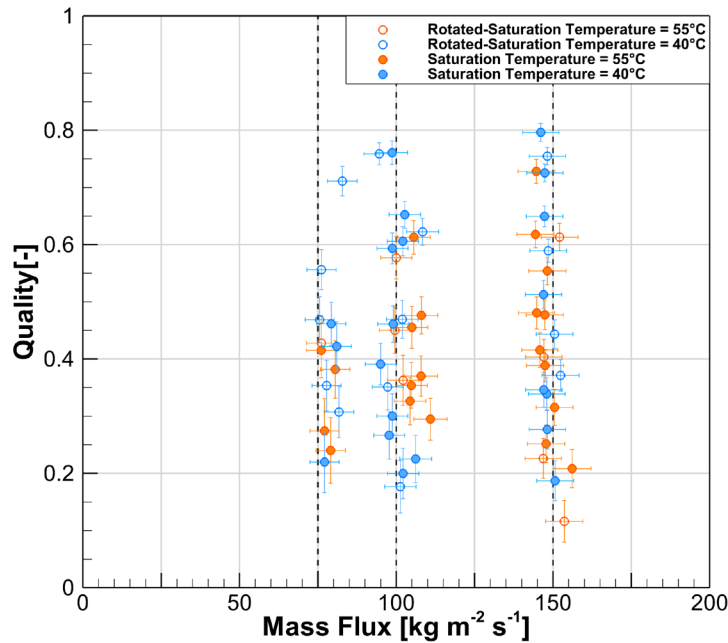

Figure 3: Data points obtained with uncertainty in mass flux and thermodynamic quality

4. Results and Discussion

Experiments were conducted at saturation temperatures of 40°C and 55°C, nominal mass fluxes from 75 to 150 kg m^{-2} s^{-1} and thermodynamic quality of 0.1 to 0.8. Data points are indicated in Figure 3. Collected data included high-speed visualization of the flow and temperature, pressure and flow rate measurements that allowed the determination of the thermodynamic quality and mass flux in the visualization section. To resolve the flow regimes, experiments were conducted with the test section in two orientations, with visualization from top (camera parallel to gravity, closed symbols in Figure 3) and with the test section rotated and visualized from the side (camera perpendicular to gravity, open symbols in Figure 3). This arrangement allowed the resolution of either annular, wavy/stratified, or intermittent type flow. As Table 1 showed previously, the channels were not exactly square, so the average aspect ratio (defined as W/H) varies from 0.92 in the top-down visualization to 1.08 in the rotated side-visualization.

4.1 Experimental Results

Based on prior work [17,27], it was expected that the observed flow regimes would be primarily annular or intermittent and that wavy/stratified flow would be absent at these flow rates and qualities. Preliminary assessment of the experimental matrix using the Nema et al. [17] flow map predicted a transition directly from annular to intermittent flow would be observed. However, for the range of conditions investigated (Figure 3), only annular or wavy/annular flow regimes were observed. Due to limitations of the optics of the present experiment, we are unable to differentiation between wavy/annular or pure annular. All data exhibited some degree of waviness in the liquid film. Figure 4 shows still images of the flow at $G = 100$ kg m^{-2} s^{-1} and $T_{sat} = 40$°C and three different thermodynamic qualities. The liquid volume increases at decreasing quality, but a clear transition to intermittent flow is not observed. Similar observations were made for all other data points.

At the two saturation temperatures tested, the different fluid properties may affect the flow regime. Moving from $T_{sat} = 40$°C to 55°C, the liquid viscosity decreases 18%, and the vapor density increases 52%. The vapor viscosity and liquid density stay relatively the same, with changes under 8%. Figure 5 compares
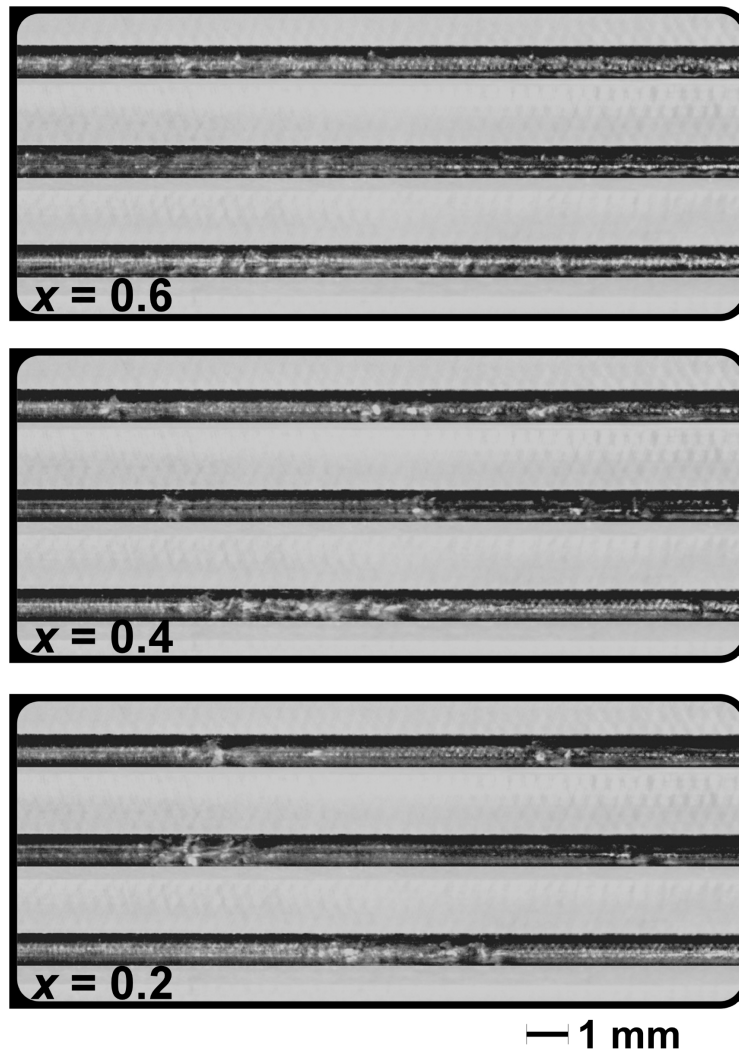
Figure 4: Comparison of visualization results at $G = 100$ kg m^{-2} s^{-1}, $T_{\text{sat}} = 40°C$, and three different thermodynamic qualities

the effect of differing saturation temperature between two data points at the same nominal average quality ($x = 0.2$) and mass flux ($G = 150$ kg m^{-2} s^{-1}). For these points, the observed flow regime is the same (annular/wavy). Intermittent flow was not observed for either saturation temperature.

Both Figure 4 and 5 were captured with the camera from above the test section, suggesting that the flow could be either annular or wavy/stratified. When the same data point were repeated with the test section rotated, it was confirmed that the flow regime was a wavy/annular type flow. For a clearer interpretation of the data, videos have been made publically available here [28].
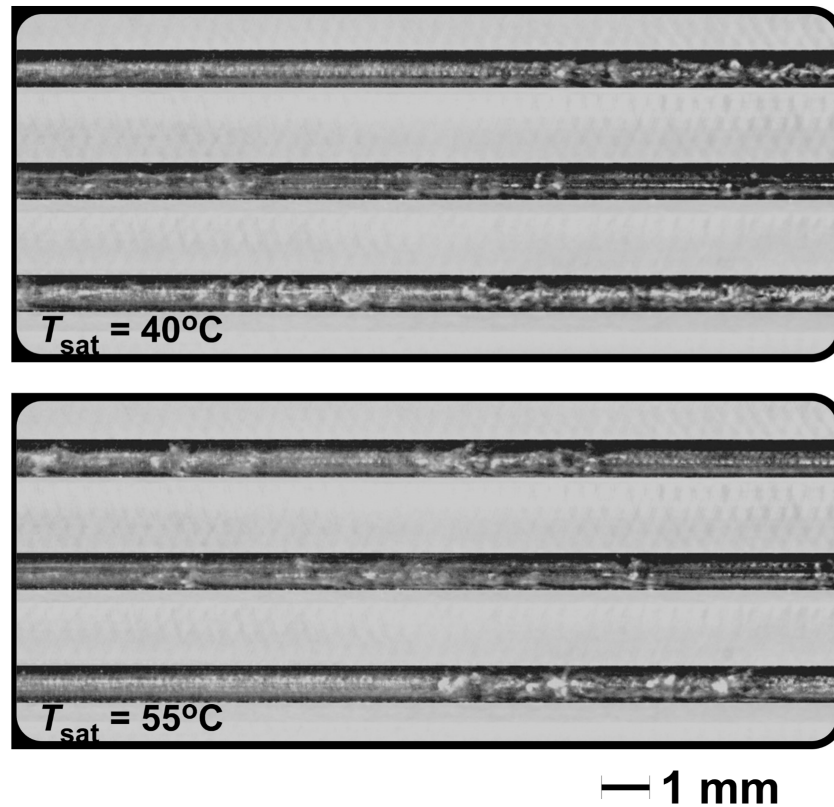
Figure 5: Comparison of visualization results at $G = 100$ kg m^{-2} s^{-1}, $x = 0.2$, and two saturation temperatures

4.2 Comparison with Literature

The collected data was compared to the predictions of several flow maps for two-phase flows in macro- and mini/microchannels. The first maps considered was the classical Taitel and Dukler [12] flow map developed based on a set of five dimensionless parameters that capture the relative effects of liquid-vapor mass flow rates, tube diameter and inclination, and fluid properties (neglecting surface tension). The collected data was plotted against the transition criteria, shown in Figure 6. The model correctly predicts 98% of the data points collected to be annular flow.

The flow regime prediction model proposed by Cavallini et al. [1] for refrigerants in round macro tubes uses the dimensionless vapor velocity, j_v*, to determine a transition line above which all flow becomes annular. Additionally, the model relies on the modified Martinelli parameter X_{tt}, as well as the critical mass flux G_W, as defined by [29]. The parameters used in the model are defined below.
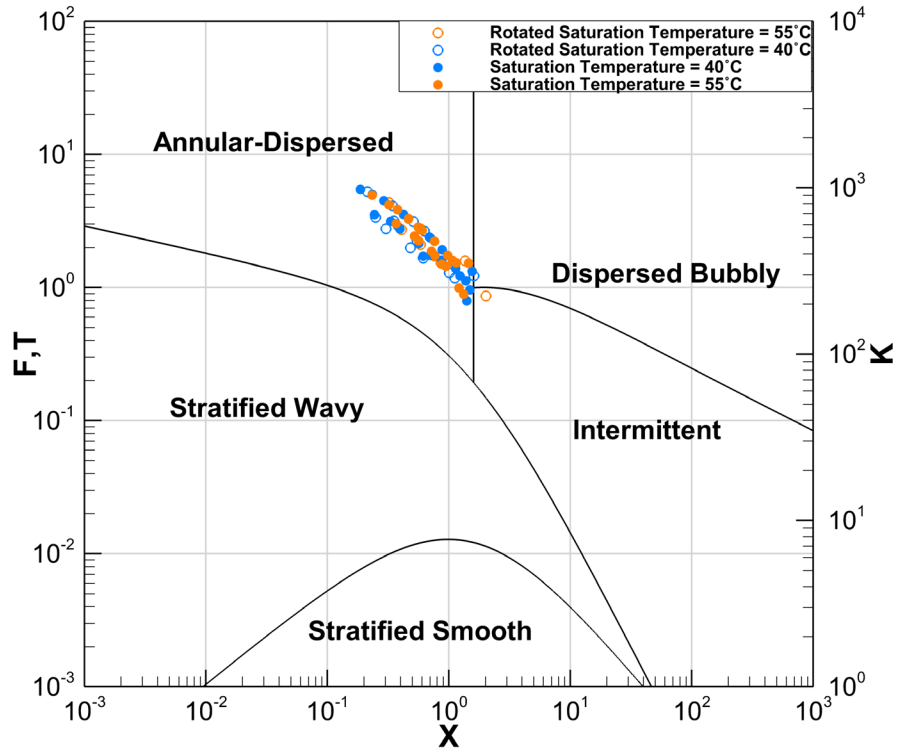
Figure 6: Experimental results compared with Taitel and Dukler {Formatting Citation} flow map

$$j_v^* = \frac{Gx}{\left(gD\rho_V\left(\rho_L - \rho_V\right)\right)^{0.5}} \tag{6}$$

$$X_{tt} = \left(\frac{\mu_L}{\mu_V}\right)^{0.1}\left(\frac{\rho_V}{\rho_L}\right)^{0.5}\left(\frac{1-x}{x}\right)^{0.9} \tag{7}$$

$$G_W = \left(\pi/4\right)Fr\sqrt{g}\rho_L D_H^{1.5} \tag{8}$$

The model was fit to specific values of these parameters as transition lines, which were used to define

flow regimes bounded by the transitions, with criteria in Table 2. Comparing the predictions of the Cavallini

et al. [1] model with the experimental conditions, 2% of the data is predicted to be intermittent, 64% wavy,

and 34% annular. Representative results for a saturation temperature of 40°C are shown in Figure 7. Unlike

flow maps developed for smaller channels, the Cavallini et al. [1] map predicts a transition from annular to

wavy to intermittent.

Table 2: Flow transition criteria of Cavallini et al. [1]

Flow Regime	Transition Criteria
Annular	$j_v \geq 2.5$, $X_{tt} < 1.6$
Wavy	$j_v < 2.5$, $X_{tt} < 1.6$
Intermittent	$j_v < 2.5$, $X_{tt} > 1.6$, $G > G_W$
Stratified	$j_v < 2.5$, $X_{tt} > 1.6$, $G < G_W$
Dispersed	Annular, $X_{tt} \gg 1.6$

The El Hajal et al. [14] flow map was developed for condensation of refrigerant in round macroscale tubes. The transition lines are presented as the transition mass flux as a function of (among many other parameters) the fluid quality x. Figure 8 shows below show the comparison between the data collected and modeled expectations as predicted by El Hajal et al. [14] for a saturation temperature of 40°C. The El Hajal et al. [14] flow map predicts nearly all data points observed in this study to be within the stratified flow regime. From the data, it was visually apparent that the flows were clearly not smooth, stratified flows.
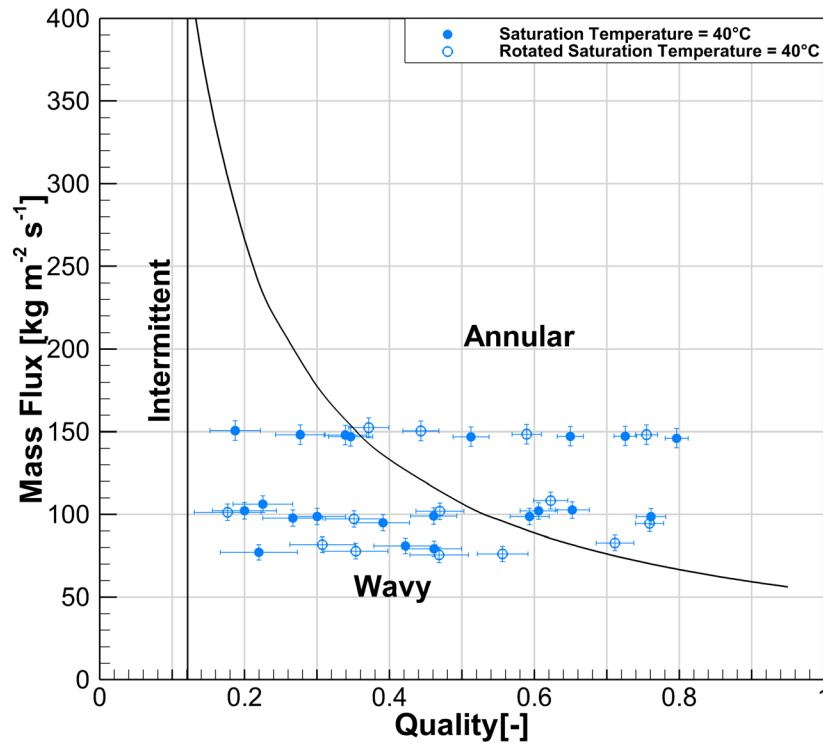

Figure 7: Experimental data at $T_{sat} = 40°C$ compared with transition criteria of Cavallini et al. [1]

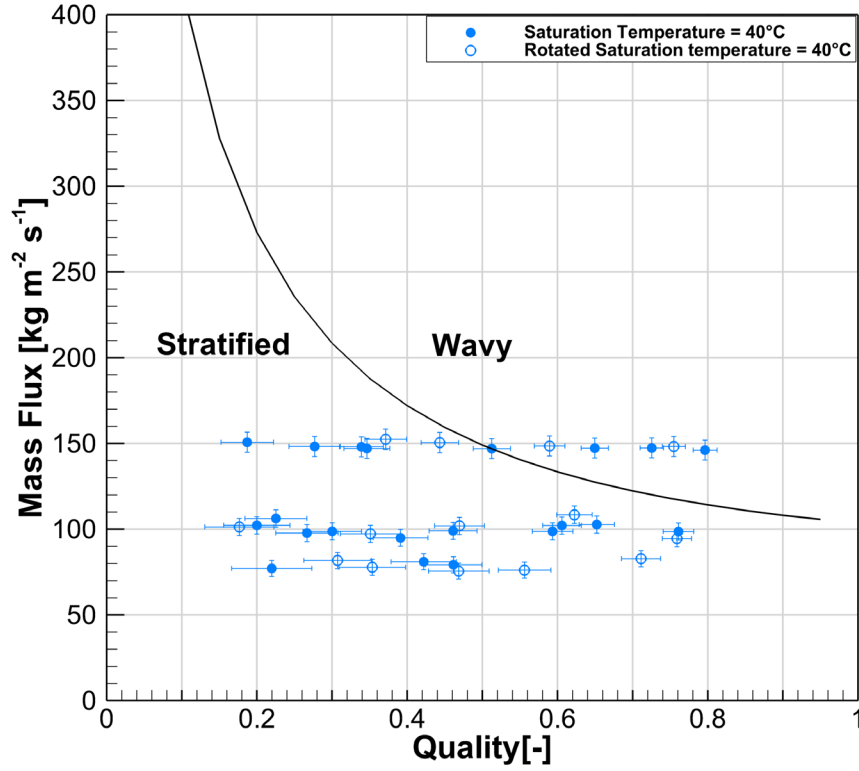Figure 8: Experimental data at $T_{sat} = 40°C$ compared with transition criteria of El Hajal et al. [14]

Thus, the flow map presented by El Hajal et al. [14] does not accurately predict any of the experimental dataset collected well.

Two sets of flow transition criteria developed for refrigerants in round and rectangular mini/microchannels were considered. The flow transition criteria (Table 3) proposed by Kim and Mudawar [16] uses a modified Weber number (Eq. (9)) and the turbulent-turbulent Martinelli parameter to fit dimensionless curves to a wide range of data from numerous researchers.

$$We^* = \begin{cases} 2.45 \dfrac{Re_V^{0.64}}{Su_V^{0.3}\left(1+1.09X_{tt}^{0.039}\right)^{0.4}} & for\ Re_L \leq 1250 \\[4mm] 0.85 \dfrac{Re_V^{0.79}\ X_{tt}^{0.157}}{Su_V^{0.3}\left(1+1.09X_{tt}^{0.039}\right)^{0.4}}\left[\left(\dfrac{\mu_V}{\mu_L}\right)^2\left(\dfrac{v_V}{v_L}\right)\right]^{0.084} & for\ Re_L > 1250 \end{cases} \tag{9}$$

Table 3: Flow transition criteria from Kim and Mudawar [16]

Flow Regime	Transition Criteria
Annular	$We > 90X_{tt}^{0.5}$
Wavy-Annular	$24X_{tt}^{0.41} < We < 90X_{tt}^{0.5}$
Transition (A-I)	$7X_{tt}^{0.2} < We < 24X_{tt}^{0.41}$
Intermittent	$We < 7X_{tt}^{0.2}$

A comparison between experimental data and the predictions made by the Kim and Mudawar [16] model is shown for $T_{sat} = 40°C$ in Figure 9. Note that due to the bounds of the plots, the annular region of the model is not visible. Nearly all of the data points captured by the present study were expected to be well within the intermittent flow regime. The wavy bend seen in the transition criteria occurring around a quality of 0.3 in both graphs represents the transition region where $Re_L = 1250$, and the transition undergoes a slight discontinuity – shown in the graph as a continuous line.

Finally, the flow map proposed by Nema et al. [17] uses the Martinelli parameter, Bond number, Weber number, and dimensionless variable T proposed by Taitel and Dukler [12] to predict flow regimes in micro and macro scale channels. The map uses the critical Bond number, defined by Equation (10) below, as a criterion to distinguish between large and small channels, defining where surface tension effects begin to play a significant role in the observed flow regime. The microscale regimes predicted by the Nema et al. [17] flow map are dispersed, annular, intermittent, and mist.

$$Bo_{crit} = \frac{1}{\left(\dfrac{\rho_L}{\rho_L - \rho_V} - \dfrac{\pi}{4} \right)} \tag{10}$$
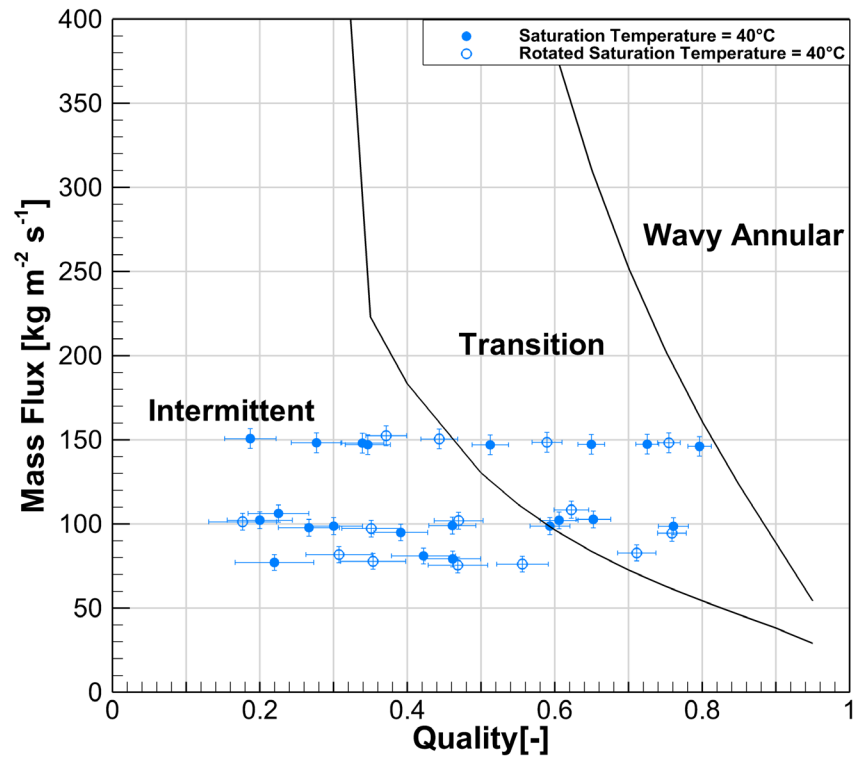
Figure 9: Experimental data at $T_{sat} = 40°C$ compared with transition criteria of Kim and Mudawar [16]

The transition criteria for flows in the microscale regime are shown in Table 4, and are a functions of the vapor-phase weber number (We_v), modified Martinelli parameter (X_{tt}), and T parameter as defined by Taitel and Dukler [12].

Calculation of the Bond number and critical Bond number for the data in this study show it to be well within the "microscale" as defended by the Nema et al. flow model. Selecting an example data point ($T_{sat} = 40.84°C$, $x = 0.57$, $G = 102$ kg m^{-2} s^{-1}), with vapor and liquid densities of 51.33 and 1143 kg m^{-3} respectively, the critical Bond number is calculated to be 3.822 via Equation (10), compared to an actual Bond number of 1.265 for this point. The same was shown to be true of all data points collected.

Knowing that the dataset is operating in the microscale regime, the remainder of the necessary dimensionless parameters were calculated and compared to the model to make predictions on the expected flow regime of each datapoint. The predictions for the data at $T_{sat} = 40°C$ are shown below in Figure 10.

Table 4: Microchannel Flow transition criteria from Nema et al. [17]

Flow Regime	Transition Criteria
Mist	$We_v > 700$, $X_{tt} < 0.175$
Dispersed	$We_v < 35$, $X_{tt} > 0.3521$, and $T_G \geq T_{trans}$
Annular	Mist and Dispersed flow are not present, $X_{tt} > 0.3521$, and any We_v
Transition (A-I)	$6 \leq We_v < 35$, $X_{tt} > 0.3521$, and Dispersed flow is not present
Intermittent	$We_v < 6$, $X_{tt} > 0.3521$, and Dispersed flow is not present

The model predicted a large percentage (46% for $T_{sat} = 40°C$ and 63% for $T_{sat} = 55°C$) of the data to be within the intermittent regime, as was originally expected during the development of the present study.

The maps evaluated predicted flow to be stratified, wavy, annular, intermittent or dispersed. Many of the flow maps predicted some percentage of the points to be intermittent or purely wavy flow, as shown in
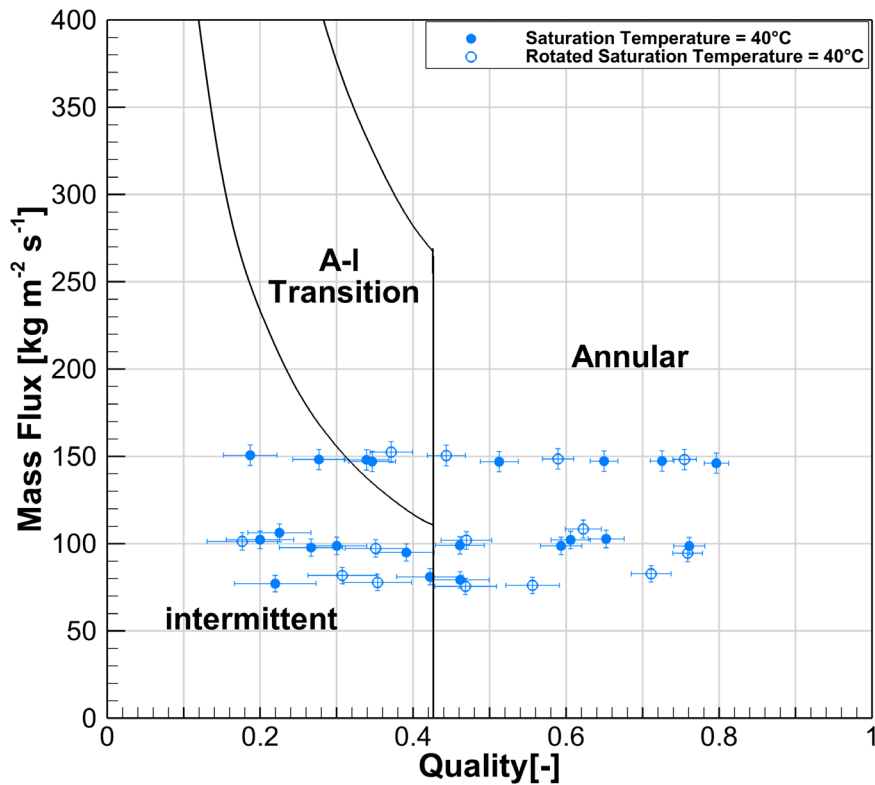

Figure 10: Experimental data at $T_{sat} = 40°C$ compared with transition criteria of Nema et al. [17]

Table 5. As evident by the photo and video data [28], there were no data points clearly in the intermittent flow regime nor purely wavy regime. This over prediction of intermittent and wavy flow is important, as the heat transfer and pressure drop mechanisms for intermittent and wavy versus annular flow are significantly different, and different types of mechanistic models would be developed and used.

There are several possible explanations for the apparent disagreement between data and models. The channels were square rather than round. The presence of sharp corners could retain liquid due to surface tension and prevent the formation of liquid bridges, which eventually cause the transition to intermittent flow. Thus, it is perhaps not surprising that the models developed for condensation in larger, circular tubes [1,14] did not predict well. However, the two mini/microchannel maps [16,17] did include data for condensing refrigerants in non-circular tubes. Several factors may contribute to the discrepancy between the mini/microchannel maps and the data. While the Nema et al. flow map was developed from R-134a data, there was no data at the combination of low mass flux and small hydraulic diameter characteristic of this study. Similarly, the Kim and Mudawar study was based on 923 mini/microchannel condensation data points for circular and non/circular channels from 0.96 mm to 3.25 mm. Of the data they considered, 23% were non-annular flow, however the minimum mass flux at the smallest hydraulic diameter of the studies considered was not reported. In the present study, the top plate is made of a polycarbonate while the other three channel walls are aluminum, which may lead to different wetting characteristics. In addition, the channels were asymmetrically cooled from the bottom with fin-effects on the sidewall. It is unclear what impact non-uniform wetting and asymmetric cooling may have on flow transitions for these conditions. Finally, there is the possibility that non-equilibrium effects are important. The data are all reported at thermodynamic equilibrium qualities. Recent work by Liang et al. [30] suggest that there can be a large deviation between thermodynamic equilibrium quality and actual vapor quality at low qualities due to subcooling. This can distort predictions made at low vapor qualities and likely contributes to the scatter in the literature. Developing more advanced flow maps that account for non-equilibrium effects may be necessary to more accurately capture transition behavior in mini/microchannel flows. Finally, it is also

interesting to note that none of the models exhibited particularly good agreement with one another for the range of conditions considered in this study. These results suggest that further work is required to refine flow transition criteria of refrigerants at low mass fluxes.

5. Conclusions

In the present study, a test bed was developed capable of high-speed visualization and measurement of two-phase fluid refrigerant flow through microchannels at low mass fluxes. The test bed was used to collect data ($75 < G < 150$ kg m^{-2} s^{-1}, $0.05 < x < 0.75$, $D_h = 0.84$ mm) at two different saturation temperatures (T_{sat} = 40, 55°C) to assess the predicative capability of a variety of flow maps when applied to fluid flow in microchannels at such low mass fluxes. While the visualization was done under locally adiabatic conditions, the flow was condensed from a superheated state in a continuous microchannel rather than boiled or introduced as two-phase mixture, providing a better representation of what would happen in an actual condenser.

The flow regimes observed for the range of conditions was primarily annular or wavy/annular flow. Transition to intermittent or wavy flow was not observed. Flow results were compared to flow maps presented by a variety of authors for macro and mini/microchannels, with none of the maps predicting the data well. Of the maps considered, the Taitel and Dukler [12] map surprisingly performed the best, correctly predicting 98% of the data to be annular and the rest intermittent. The Nema et al. [17] map was a distant second, predicting 46% as annular, with the remainder intermittent. Even though developed from data for

Table 5: Summary of flow regime predictions by maps evaluated

Proposed Model	Percent of data predicted to be within designated flow regime					
	Stratified	Wavy	Annular	Intermittent	Dispersed	Mist
Taitel and Dukler [12]	0%	0%	98%	2%	0%	0%
Cavallini et al. [1]	0%	64%	34%	2%	0%	0%
El Hajal et al. [15]	88%	12%	0%	0%	0%	0%
Kim and Mudawar [16]	0%	0%	0%	100%	0%	0%
Nema et al. [17]	0%	0%	46%	54%	0%	0%

small channels, the Nema et al. [17] map did not include data for channels below 1 mm or such low mass fluxes. Also of interest is that none of the maps agreed particularly well with one another. Potential reasons for discrepancy between the data and predictions include the use of non-circular tubes (stronger surface tension effects), operation at conditions outside the range, particularly the low mass flow for which most maps were developed for, as well as the potential for non-equilibrium effects at low mass flux and low thermodynamic quality. The results suggest that further work to understand flow transitions at low mass flux in small, non-circular channels are required. Understanding these transitions is critical to developing mechanistic heat transfer and pressure drop models for design of microchannel based condensers.

Acknowledgments

References

[1]   A. Cavallini, G. Censi, D. Del Col, L. Doretti, G. Longo, L. Rossetto, Condensation of Halogenated Refrigerants Inside Smooth Tubes, HVAC&R Res. 8 (2002) 429–451. doi:10.1080/10789669.2002.10391299.

[2]   R. Revellin, V. Dupont, T. Ursenbacher, J.R. Thome, I. Zun, Characterization of diabatic two-phase flows in microchannels: Flow parameter results for R-134a in a 0.5 mm channel, Int. J. Multiph. Flow. 32 (2006) 755–774. doi:10.1016/j.ijmultiphaseflow.2006.02.016.

[3]   E. Rahim, R. Revellin, J. Thome, A. Bar-Cohen, Characterization and prediction of two-phase flow regimes in miniature tubes, Int. J. Multiph. Flow. 37 (2011) 12–23. doi:10.1016/j.ijmultiphaseflow.2010.09.002.

[4]   J. Coleman, S. Garimella, Two-phase flow regimes in round, square and rectangular tubes during condensation of refrigerant R134a, Int. J. Refrig. 26 (2003) 117–128. doi:http://dx.doi.org/10.1016/S0140-7007(02)00013-0.

[5]   C.-Y. Yang, C.-C. Shieh, Flow pattern of air–water and two-phase R-134a in small circular tubes, Int. J. Multiph. Flow. 27 (2001) 1163–1177. doi:10.1016/S0301-9322(00)00070-7.

[6]   C.L. Ong, J.R. Thome, Macro-to-microchannel transition in two-phase flow: Part 1 – Two-phase flow patterns and film thickness measurements, Exp. Therm. Fluid Sci. 35 (2011) 37–47. doi:10.1016/j.expthermflusci.2010.08.004.

[7]   S. Garimella, B.M. Fronk, Encyclopedia of Two-Phase Heat Transfer and Flow I: Fundamentals and Methods Volume 2: Condensation Heat Transfer, 1st ed., World Scientific Publishing Co., 2015.

[8]   L. Doretti, C. Zilio, S. Mancin, A. Cavallini, Condensation flow patterns inside plain and microfin tubes: A review, Int. J. Refrig. 36 (2013) 567–587. doi:10.1016/j.ijrefrig.2012.10.021.

[9]   J.R. Thome, Boiling in microchannels: A review of experiment and theory, Int. J. Heat Fluid Flow. 25 (2004) 128–139. doi:10.1016/j.ijheatfluidflow.2003.11.005.

[10]   C.B. Tibiriçá, G. Ribatski, Flow boiling in micro-scale channels – Synthesized literature review, Int. J. Refrig. 36 (2013) 301–324. doi:10.1016/j.ijrefrig.2012.11.019.

[11]   B.M. Fronk, K.R. Zada, Evaluation of Heat and Mass Transfer Models for Sizing Low-Temperature Kalina Cycle Microchannel Condensers, J. Energy Resour. Technol. 139 (2016) 22002. doi:10.1115/1.4034229.

[12]   Y. Taitel, A.E. Dukler, A model for predicting flow regime transitions in horizontal and near horizontal gas-liquid flow, AIChE J. 22 (1976) 47–55. doi:10.1002/aic.690220105.

[13]   N. Kattan, J.R. Thome, D. Favrat, Flow Boiling in Horizontal Tubes: Part 1—Development of a Diabatic Two-Phase Flow Pattern Map, J. Heat Transfer. 120 (1998) 140. doi:10.1115/1.2830037.

[14]   J. El Hajal, J.. Thome, A. Cavallini, Condensation in horizontal tubes, part 1: two-phase flow pattern map, Int. J. Heat Mass Transf. 46 (2003) 3349–3363. doi:10.1016/S0017-9310(03)00139-X.

[15]   J.R. Thome, J. El Hajal, A. Cavallini, Condensation in horizontal tubes, part 2: new heat transfer model based on flow regimes, Int. J. Heat Mass Transf. 46 (2003) 3365–3387. doi:10.1016/S0017-9310(03)00140-6.

[16]   S.M. Kim, I. Mudawar, Flow condensation in parallel micro-channels - Part 2: Heat transfer results and correlation technique, Int. J. Heat Mass Transf. 55 (2012) 984–994. doi:10.1016/j.ijheatmasstransfer.2011.10.012.

[17]   G. Nema, S. Garimella, B.M. Fronk, Flow regime transitions during condensation in microchannels, Int. J. Refrig. 40 (2014) 227–240. doi:10.1016/j.ijrefrig.2013.11.018.

[18]   V.G. Niño, P.S. Hrnjak, T.A. Newell, Two-Phase Flow Visualization of R134A in a Multiport Microchannel Tube, Heat Transf. Eng. 24 (2003) 41–52. doi:10.1080/01457630304042.

[19]   A. Kawahara, P.M.-Y. Chung, M. Kawaji, Investigation of two-phase flow pattern, void fraction and pressure drop in a microchannel, Int. J. Multiph. Flow. 28 (2002) 1411–1435. doi:10.1016/S0301-9322(02)00037-X.

[20]   J.W. Coleman, S. Garimella, Characterization of two-phase flow patterns in small diameter round and rectangular tubes, Int. J. Heat Mass Transf. 42 (1999) 2869–2881. doi:10.1016/S0017-9310(98)00362-7.

[21]   P.A. Kew, K. Cornwell, Correlations for the prediction of boiling heat transfer in small-diameter channels, Appl. Therm. Eng. 17 (1997) 705–715. doi:10.1016/S1359-4311(96)00071-3.

[22]   National Instruments, LabVIEW, (2016).

[23]   S.A. Klein, Engineering Equation Solver, (2015).

[24]   R. Tillner-Roth, H.D. Baehr, An International Standard Formulation for the Thermodynamic Properties of 1,1,1,2-Tetrafluoroethane (HFC-134a) for Temperatures from 170 K to 455 K and Pressures up to 70 MPa, J. Phys. Chem. Ref. Data. 23 (1994) 657–729. doi:10.1063/1.555958.

[25]   M.A. VanderPutten, Evaluation of the Predictive Capability of Two-Phase Flow Maps for Microchannel Condensation of R-134a at Low Mass Flux Conditions, Oregon State University, 2017. http://hdl.handle.net/1957/61677.

[26]   S.J. Kline, F.A. McClintock, Describing Uncertainties in Single Sample Experiments, Mech. Eng. (1953).

[27]   J.W. Coleman, S. Garimella, Visualization of Refrigerant Two-Phase Flow During Condensation, in: 34th Natl. Heat Transf. Conf., ASME, Pittsburgh, PA, USA, 2000.

[28]   T.A. Jacob, M. Sattar, N. Ali, B.M. Fronk, Flow visualization of R-134a at mass fluxes form 75 to 150 kg m^{-2} s^{-1}, for a quality from 0.1 to 0.8 in square, parallel microchannels (D = 0.84 mm), (2017). https://doi.org/10.6084/m9.figshare.5248390.v2.

[29]   T.J. Rabas, B. Arman, Effect of the Exit Condition on the Performance of In-Tube Condensers, Heat Transf. Eng. 21 (2000) 4–14. doi:10.1080/014576300271112.

[30]   G. Liang, N. Mascarenhas, I. Mudawar, Analytical and experimental determination of slug flow parameters, pressure drop and heat transfer coefficient in micro-channel condensation, Int. J. Heat Mass Transf. 111 (2017) 1218–1233. doi:10.1016/j.ijheatmasstransfer.2017.04.045.